Sub-diffraction-limited fluorescent patterns by tightly focusing polarized femtosecond vortex beams in a silver-containing glass References and links

Eungjang Lee, Yannick Petit, Etienne Brasselet, Thierry Cardinal, Seung-Han P Park, Lionel Canioni

Sub-diffraction-limited fluorescent patterns by tightly focusing polarized femtosecond vortex beams in a silver-containing glass

EUNGJANG LEE,[1] YANNICK PETIT,[1,2,*] ETIENNE BRASSELET,[3,4] THIERRY CARDINAL,[2] SEUNG-HAN PARK,[5] AND LIONEL CANIONI[1]

[1]*University of Bordeaux, CNRS, CEA, CELIA, UMR 5107, F-33405 Talence, France*
[2]*University of Bordeaux, CNRS, ICMCB, UPR 9048, F-33608 Pessac, France*
[3]*University of Bordeaux, LOMA, UMR 5798, F-33400 Talence, France*
[4]*CNRS, LOMA, UMR 5798, F-33400 Talence, France*
[5]*Yonsei University, Department of Physics, 120-749 Seoul, South Korea*
[*]*Yannick.petit@u-bordeaux.fr*

Abstract: We report that the shape and size of fluorescent patterns can be controlled by the focused laser intensity distribution, which depends on irradiation conditions as well as on the spin and orbital angular momenta being carried by light, inducing the formation of silver cluster patterns in a silver-containing zinc phosphate glass. In particular, we demonstrate that sub-diffraction-limited inner structures of fluorescent patterns can be generated by direct laser writing (DLW) with tightly focused femtosecond laser vortex beams as Laguerre-Gauss modes (LG_0^1) with linear and left-handed circular polarizations. We believe this technique, further combined with dual-color DLW, can be useful and powerful for developing structured light enabled nanostructures.

OCIS codes: (140.3390) Laser materials processing; (140.3300) Laser beam shaping; (080.4865) Optical vortices; (190.4180) Multiphoton processes; (050.6624) Subwavelength structures.

References and links

1. L. Allen, M. W. Beijersbergen, R. J. C. Spreeuw, and J. P. Woerdman, "Orbital angular momentum of light and the transformation of Laguerre-Gaussian laser modes," Phys. Rev. A **45**(11), 8185–8189 (1992).
2. A. M. Yao and M. J. Padgett, "Orbital angular momentum: origins, behavior and applications," Adv. Opt. Photonics **3**(2), 161–204 (2011).
3. M. Padgett and R. Bowman, "Tweezers with a twist," Nat. Photonics **5**(6), 343–348 (2011).
4. J. Hamazaki, R. Morita, K. Chujo, Y. Kobayashi, S. Tanda, and T. Omatsu, "Optical-vortex laser ablation," Opt. Express **18**(3), 2144–2151 (2010).
5. C. Hnatovsky, V. G. Shvedov, W. Krolikowski, and A. V. Rode, "Materials processing with a tightly focused femtosecond laser vortex pulse," Opt. Lett. **35**(20), 3417–3419 (2010).
6. K. Mishchik, Y. Petit, E. Brasselet, A. Royon, T. Cardinal, and L. Canioni, "Patterning linear and nonlinear optical properties of photosensitive glasses by femtosecond structured light," Opt. Lett. **40**(2), 201–204 (2015).
7. J. Fischer and M. Wegener, "Three-dimensional optical laser lithography beyond the diffraction limit," Laser Phys. Rev. **7**(1), 22–44 (2013).
8. Z. Gan, Y. Cao, R. A. Evans, and M. Gu, "Three-dimensional deep sub-diffraction optical beam lithography with 9 nm feature size," Nat. Commun. **4**, 2061 (2013).
9. J. Kaschke and M. Wegener, "Gold triple-helix mid-infrared metamaterial by STED-inspired laser lithography," Opt. Lett. **40**(17), 3986–3989 (2015).
10. C. Hnatovsky, V. G. Shvedov, N. Shostka, A. V. Rode, and W. Krolikowski, "Polarization-dependent ablation of silicon using tightly focused femtosecond laser vortex pulses," Opt. Lett. **37**(2), 226–228 (2012).
11. O. J. Allegre, W. Perrie, S. P. Edwardson, G. Dearden, and K. G. Watkins, "Laser microprocessing of steel with radially and azimuthally polarized femtosecond vortex pulses," J. Opt. **14**(8), 085601 (2012).
12. M. Bellec, A. Royon, K. Bourhis, J. Choi, B. Bousquet, M. Treguer, T. Cardinal, J.-J. Videau, M. Richardson, and L. Canioni, "3D patterning at the nanoscale of fluorescent emitters in glass," J. Phys. Chem. C **114**(37), 15584–15588 (2010).
13. L. Canioni, M. Bellec, A. Royon, B. Bousquet, and T. Cardinal, "Three-dimensional optical data storage using third-harmonic generation in silver zinc phosphate glass," Opt. Lett. **33**(4), 360–362 (2008).

14. J. Choi, M. Bellec, A. Royon, K. Bourhis, G. Papon, T. Cardinal, L. Canioni, and M. Richardson, "Three-dimensional direct femtosecond laser writing of second-order nonlinearities in glass," Opt. Lett. **37**, 1029–1031 (2012).
15. G. Papon, Y. Petit, N. Marquestaut, A. Royon, M. Dussauze, V. Rodriguez, T. Cardinal, and L. Canioni, "Fluorescence and second-harmonic generation correlative microscopy to probe space charge separation and silver cluster stabilization during direct laser writing in a tailored silver-containing glass," Opt. Mater. Express **3**(11), 1855–1861 (2013).
16. G. Papon, N. Marquestaut, Y. Petit, A. Royon, M. Dussauze, V. Rodriguez, T. Cardinal, and L. Canioni, "Femtosecond single-beam direct laser poling of stable and efficient second-order nonlinear optical properties in glass," J. Appl. Phys. **115**(11), 113103 (2014).
17. N. Marquestaut, Y. Petit, A. Royon, T. Cardinal, and L. Canioni, "Three-dimensional silver nanoparticles formation using femtosecond laser irradiation in phosphate glasses: analogy with photography," Adv. Funct. Mater. **24**, 5824–5832 (2014).
18. S. Danto, F. Désévédavy, Y. Petit, J.-C. Desmoulin, A. Abou Khalil, C. Strutynski, M. Dussauze, F. Smektala, T. Cardinal, and L. Canioni, "Photo-inscriptible silver-containing phosphate glass ribbon fibers," Adv. Opt. Mater. **4**(1), 162–168 (2016).
19. J.-M. Guay, A. Villafranca, F. Baset, K. Popov, L. Ramunno, and V. R. Bhardwaj, "Polarization-dependent femtosecond laser ablation of poly-methyl methacrylatsze," New J. Phys. **14**(8), 085010 (2012).
20. C. Hnatovsky, V. G. Shvedov, and W. Krolikowski, "The role of light-induced nanostructures in femtosecond laser micromachining with vector and scalar pulses," Opt. Express **21**(10), 12651–12656 (2013).
21. X. Li, W. Rong, L. Jiang, K. Zhang, C. Li, Q. Cao, G. Zhang, and Y. Lu, "Generation and elimination of polarization-dependent ablation of cubic crystals by femtosecond laser radiation," Opt. Express **22**(24), 30170–30176 (2014).
22. N. Matsumoto, T. Ando, T. Inoue, Y. Ohtake, N. Fukuchi, and T. Hara, "Generation of high-quality higher-order Laguerre-Gaussian beams using liquid-crystal-on-silicon spatial light modulators," J. Opt. Soc. Am. A **25**(7), 1642–1651 (2008).
23. S. N. Khonina, "Simple phase optical elements for narrowing of a focal spot in high-numerical-aperture conditions," Opt. Eng. **52**(9), 091711 (2013).
24. B. Richards and E. Wolf, "Electromagnetic diffraction in optical systems. ii. structure of the image field in an aplanatic system," Proc. R. Soc. Lond. A Math. Phys. Sci. **253**(1274), 358–379 (1959).
25. E. Smetanina, B. Chimier, Y. Petit, N. Varkentina, E. Fargin, L. Hirsch, T. Cardinal, L. Canioni, and G. Duchateau, "Modeling of cluster organization in metal-doped oxide glasses irradiated by a train of femtosecond laser pulses," Phys. Rev. A **93**(1), 013846 (2016).
26. J. Hering, E. H. Waller, and G. Von Freymann, "Automated aberration correction of arbitrary laser modes in high numerical aperture systems," Opt. Express **24**(25), 28500–28508 (2016).
27. Y. Petit, K. Mishchik, N. Varkentina, N. Marquestaut, A. Royon, I. Manek-Hönninger, T. Cardinal, and L. Canioni, "Dual-color control and inhibition of direct laser writing in silver-containing phosphate glasses," Opt. Lett. **40**(17), 4134–4137 (2015).

1. Introduction

The properties and applications of optical vortex beams have been extensively investigated because of their potential to various applications, as *e.g.* optical tweezing or efficient laser ablation [1–4]. Direct laser writing (DLW) and processing techniques with femtosecond vortex beams have been also demonstrated to overcome limitations of accessible topologies with Gaussian beams [5,6]. Super-resolution optical STED-like lithography has recently led to remarkable nanoscale structuring in polymers [7,8] and to complex artificial architectures as chiral metamaterials [9]. However, it is still challenging to transfer such all-optical approaches in inorganic materials. In addition, even if polarization dependence of tightly focused vortex beams has already been simulated [7] or considered for material ablation [10,11], the role of the polarization state of vortex beams has not yet been investigated in transparent metal-containing glasses, which is the aim of the present work.

Transparent silver-containing phosphate glasses show outstanding photonic response for tightly focused femtosecond laser pulses. Specifically, it has been reported that three-dimensional (3D) localized fluorescent silver clusters as well as third- and second-order nonlinear optical properties can be generated in such materials by multi-pulses with TW/cm^2 peak power level [12–16]. Space-selective precipitation of metallic silver nanoparticles leading to oriented plasmonic metal/dielectric composite architectures has also been demonstrated [17]. Recently, ribbon fibers have also been inscribed in such photosensitive glasses, by keeping its full initial DLW abilities, enlarging thus its applicative potential to fiber sensing [18]. Although a laser-induced response by multi-pulse irradiation is expected to

be influenced by both intensity and polarization of the writing light [19–21], to date no distinguishable polarization dependence has been observed in the fluorescence patterns in such silver-containing glass samples. Indeed, laser-induced processes seemed to depend only on the magnitude and the distribution of the light intensity. In particular, Laguerre-Gauss(LG)-like vortex beams have been shown to lead to original fluorescent patterns, such as nested double-ring cylinders [6]. Such patterns, produced with a linear polarization, were found to be independent of the sign of the topological charge of the incident vortex beam. However, previous experimental limitations of our setup prevented to address the role of the polarization state and topological charge in a systematic manner, which is now addressed in this work.

Here, we report on fluorescent patterns in a tailored silver-containing zinc phosphate glass obtained by DLW, utilizing high numerical aperture (NA) aplanatic objective lens and vortex beams with various polarization states. In particular, we find that tightly focused femtosecond laser vortex pulses with linear and circular polarizations may generate fluorescent patterns with sub-diffraction-limited inner features while considering the relevant polarizations. Indeed, such patterns show significant differences depending on the considered polarization, which is consistent with the simulated polarization-dependent intensity distribution of the vortex beams in the focal region assuming LG incident light field on the high NA objective. This supports the fact that spin-orbit coupling effects arising in highly non-paraxial light fields, especially the structure of the longitudinal field component, play a prominent role in fine optical structuring of matter.

2. Experimental setup

Figure 1(a) displays a schematic diagram of our DLW experimental setup based on a custom-built nonlinear microscope. The linearly polarized femtosecond laser (390 fs, 1030 nm, 9.2 MHz, average power of 2.6 W, t-Pulse 200, Amplitude Systems) is incident on a liquid-crystal-on-silicon (LCOS; X10468-03, Hamamatsu Photonics) spatial light modulator (SLM) to create a position-dependent phase-shift at the beam reflected by each pixel. Figures 1(b)-1(h) shows the phase holograms to create LG_p^l beams with l = 0, 1, 2 being the azimuthal index (i.e. the topological charge of the associated optical vortex) and p = 0 the radial index. The quality of the prepared beam is ensured by using a pure phase hologram formed by adding a blazed phase grating pattern to the desired LG phase distribution [Figs. 1(e)-1(h)] [22]. The irradiation duration and transmitted irradiance are controlled by an acousto-optic modulator. A quarter wave plate is introduced for controlling the polarization state of the vortex beam.

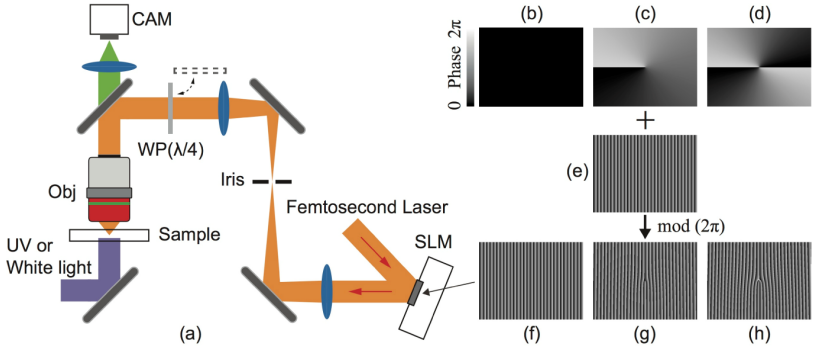

Fig. 1. (a) Experimental setup. SLM: spatial light modulator (phase-only reflective LCOS), WP: quarter-wave plate, Obj: objective lens, CAM: CCD camera. Phase holograms before (b-d) and after (f-h) adding blazed phase grating pattern (e) for generating (f) LG_0^0, (g) LG_0^1, and (h) LG_0^2 beams.

Our tailored photosensitive glass is a silver-containing zinc phosphate glass with 5% Ag_2O concentration (mol. %), prepared by a standard glass melting method and polished up to optical quality. The laser beam is focused through the microscope objective lens (MPlan N 50 × , NA 0.75, Olympus). Fluorescent images are obtained by a confocal microscope (TCS SP5, HCX PL APO CS 63 × , NA 1.4, excitation at 405 nm, emission at 440-520 nm, Leica).

3. Results

The influence of the topological charge of the writing vortex beam is explored by comparing the patterns obtained using linearly polarized LG_0^l beams with l = 0, 1 and 2. Figure 2 shows the corresponding simulated focal intensity distributions [Figs. 2(a)-2(c)], experimentally focused LG beams [Figs. 2(d)-2(f)], and created fluorescent patterns [Figs. 2(g)-2(i)]. As already reported [12], a fluorescent ring pattern composed of silver clusters [Fig. 2(g)] is formed by focusing the non-vortex LG_0^0 beam (number of pulses N = 5 × 10^7, pulse energy E_p = 13 nJ). In contrast, vortex beams LG_0^1 and LG_0^2 create unique nested double-ring patterns [Figs. 2(h) and 2(i)], for N = 5 × 10^7, $E_p = 34\,\text{nJ}$ and $50\,\text{nJ}$, respectively. Note that larger topological charges require larger incident pulse energies, which is associated with a larger spatial extent of the light field and consequently leads to larger inner/outer patterns.

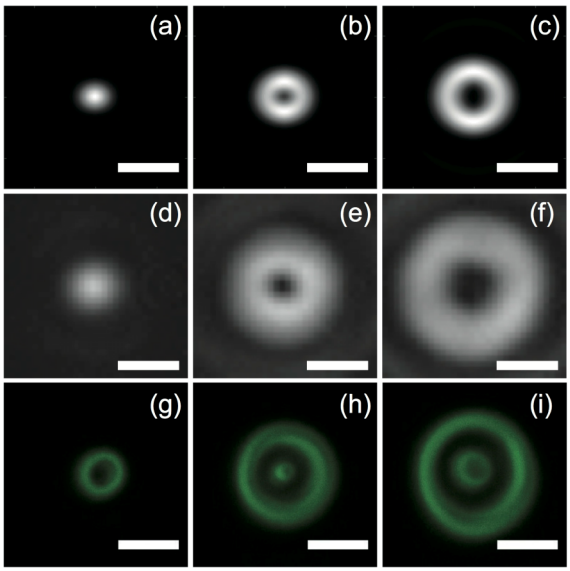

Fig. 2. Simulated intensity distributions, experimentally linearly polarized focused laser beams, and generated fluorescent patterns using (a, d, g) LG_0^0, (b, e, h) LG_0^1, and (c, f, i) LG_0^2 beams, respectively. Scale bars: 2 μm.

We also investigate the polarization influence of vortex beams on the shape and size of silver cluster distributions with identical intensity distribution at the entrance pupil of the objective lens. Recalling that the azimuthal phase distribution of LG_0^l paraxial beam of the form $e^{il\varphi}$ is associated to an orbital angular momentum per photon $l\hbar$ directed along the propagation direction, and that its polarization state is associated to a spin-angular momentum per photon of ± $\hbar$ along the propagation direction, we have selected the three following settings for the incident collimated light impinging the objective lens: (α) only the orbital angular momentum exists with no spin angular momentum; (β) the spin and orbital angular momenta are parallel, (γ) the spin and orbital angular momenta are anti-parallel [1,23,24].

Figure 3 shows the simulation of tightly focused vortices at 1030 nm, using high-aperture aplanatic lens (NA 0.75) for LG_0^1 beam with linear (Lin), left-handed circular (LHC), and right-handed circular (RHC) polarizations, which respectively refer to the cases (α, β, γ). Figures 3(a)-3(c) present the corresponding 3D intensity distributions in the focal region. Figures 3(d)-3(g) depict the cross sections of Fig. 3(a) in the focal plane (x-y plane) and through the focal plane (x-z plane). Similarly, Figs. 3(h)-3(k) and Figs. 3(l)-3(o) show the cross sections of Fig. 3(b) and Fig. 3(c), respectively. In general, the on-axis intensity distributions strongly depend on the strength and distribution of the longitudinal electric field, a well-known fact for highly non-paraxial beams [10,23].

In particular, the LHC-polarized LG_0^1 beam has zero longitudinal on-axis electric field component, resulting in zero optical intensity along the optical axis. In contrast, the RHC-polarized LG_0^1 beam has significant non-zero on-axis intensity in the focal region. Finally, as the Lin-polarized LG_0^1 beam corresponds to a linear combination of the two LHC and RHC polarized LG_0^1 beams with equal weights, it leads to an intermediate on-axis intensity distribution compared to those of the LHC and RHC ones.

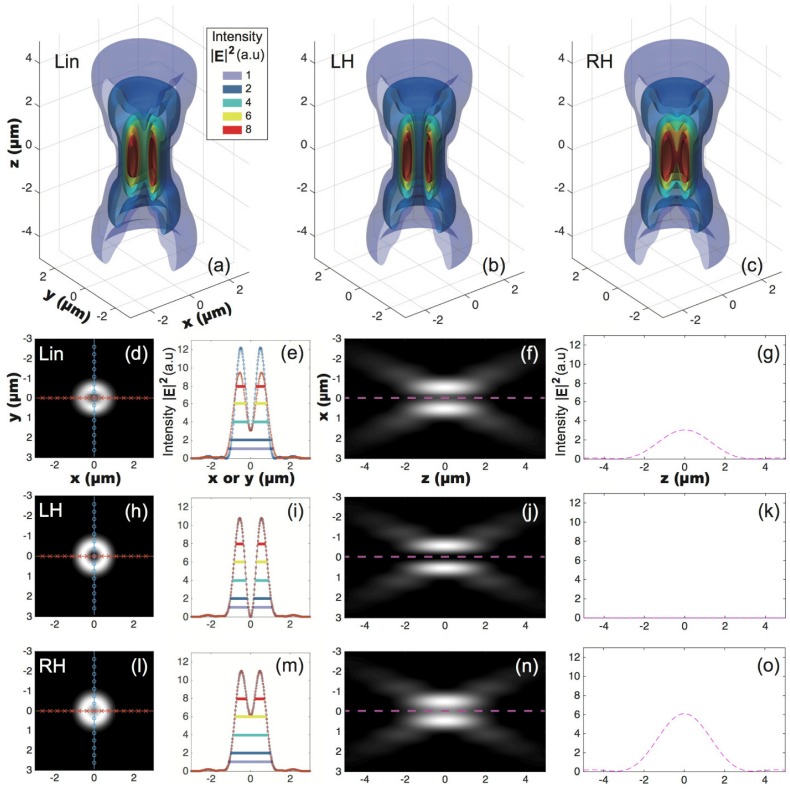

Fig. 3. Simulated focal intensity ($|E|^2$) distribution of LG_0^2 beam versus polarization. 3D iso-intensity surfaces of LG_0^2 with (a) Lin, (b) LHC, and (c) RHC polarizations. (d, h, l) Intensity distributions of (a, b c) in the focal plane. (e, i, m) Lateral intensity profiles along the horizontal/vertical directions marked in (d, h, l). (f, j, n) Intensity distributions of (a, b, c) through the focal plane. (g, k, o) On-axis intensity profiles along the dashed direction marked in (f, j, n).

The dependence of the laser induced fluorescent patterns with the irradiation parameters has been studied (Figs. 4-6). Laser parameters were $E_p = 30$, 34, and $39\,\text{nJ}$ and $N = 10^5$, 10^6

and 10^7 . Figures 4(a) and Figs. 4(b)-4(d) show the lateral and axial cross-sectional confocal images, respectively, depicting the fluorescent patterns generated by a LHC-polarized LG_0^1 beam for the different irradiation conditions. Figures 4(e) and 4(f) show the typical intensity profile of the fluorescent patterns 'iii' and 'v' of Fig. 4(a), respectively. Figure 4(e) can be well fitted with four Lorentzian functions and their peak distances are estimated to 310 ± 20 nm (inner diameter between peaks 1 and 2) and 2.12 ± 0.01 μm (outer diameter between peaks 0 and 3).

The smallest inner structure of Fig. 4(a) is obtained for 'iii' for E_p = 39 nJ and N = 10^7. Contrarily to 'v', the inner pattern 'iii' is no more transversally resolved since it appears as a single apparent peak, as shown in Figs. 4(a) and 4(f). Therefore, there are two possibilities: either this inner pattern is still a single-ring fluorescent structure (even if not resolved) or it becomes a filled fluorescent pattern. In the first hypothesis, by imposing a four-peak modeling with the same peak width parameters as those of 'v' and by allowing adjustable fitting parameters for peak positions and intensities, one estimates a sub-diffraction dimension of 185 ± 35 nm (inner diameter) and 2.33 ± 0.01 μm (outer diameter). In the hypothesis of a filled fluorescent inner pattern, the smallest inner diameter is estimated for 'iii' to be less than 390 ± 10 (FWHM). Indeed, the observed pattern is expected to be larger than the actual size since the lateral resolution of the confocal microscope was less good while imaging our structures (due to the non-matching refractive index of 1.59 of our glass) than the ideally estimated value of 220 nm by imaging sub-resolution fluorescent beads. A realistic PSF in our glass for which spherical aberrations are not ideally corrected by the imaging oil objective, should typically be 250-290 nm [6]. After a rough Gaussian deconvolution, the real diameter on the inner-structure (while supposing such fluorescent structure is filled) should be down to 260-300 nm (FWHM). Therefore, in both hypotheses, this indicates that the size of the inner fluorescent structure can be significantly smaller than 390 nm. Considering the diameter of focused Gaussian beam, ~1.5 μm under the present experimental configuration, we conclude that that LHC-polarized LG_0^1 structured light can generate sub-diffraction limited inner fluorescent patterns in the silver-containing glass.

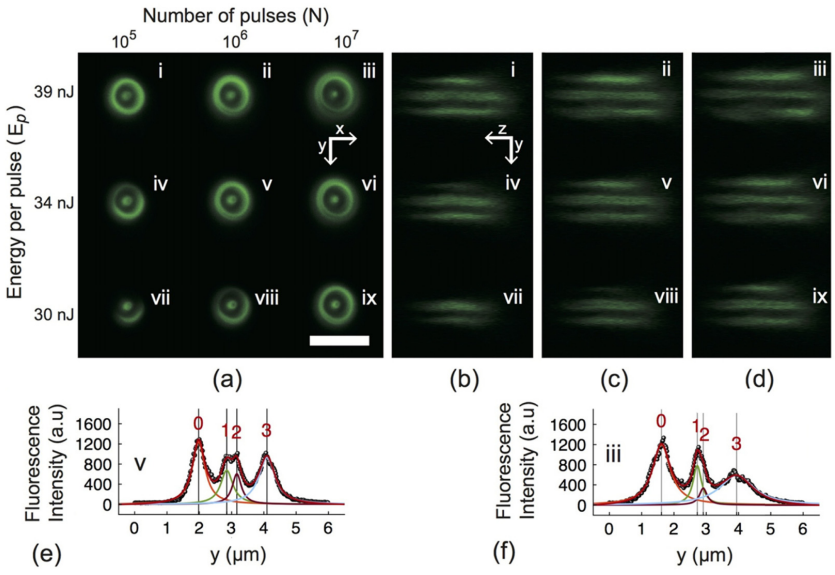

Fig. 4. Confocal image of the fluorescent patterns generated by LHC-polarized LG_0^2 beams. (a) Lateral cross-sectional images in the focal plane. (b-d) Axial cross-sectional images. (e, f) Fluorescent intensity profiles of 'v' and 'iii' along the y-axis direction. Circles and lines are experimental data and Lorentzian fitting curves. Scale bars: 4 μm.

As shown in Fig. 4, the dimensions and intensities of the fluorescent outer-ring patterns obtained by LHC-polarized LG_0^1 beams become larger with increasing the number of pulses and/or of the energy per pulse. This is consistent with the previously reported patterns obtained with Gaussian beams [12]. In contrast, the diameter of the inner-ring patterns gets smaller while increasing the irradiation parameters [Figs. 4(a), 4(e) and 4(f)]. Indeed, it becomes smaller by increasing the pulse energy at the same number of pulses since the effective inner diameters of the donut-like focused beams decrease, forcing silver ionization, silver migration and cluster creation to occur closer to the on-axis region. Similarly, cumulative effects by increasing the number of pulses also lead to smaller inner-ring patterns since multi-pulse processes push the net formation of silver clusters towards the regions of lower beam intensities, leading to the collapse of the inner-ring pattern on the on-axis region where the laser intensity is null [6,12,25]. This remarkable collapse is expected to get even stronger for objectives with higher NA, since the on-axis intensity should remain identically null.

It should be emphasized that, till now, only 0.8 μm size fluorescent patterns have been observed by DLW with focused Gaussian beams in such glasses (tightly focusing objective Plan NEO-FLUAR, 100 × , NA 1.3 oil, Zeiss). To reach the later size, laser intensity had to be decreased and the objective NA had to be increased. Besides, a micron-size fluorescent filled ring had also been reported while structuring at the material threshold [12], but such filled pattern was unstable and weak. Thus, present results obtained from LHC-polarized LG_0^1 beam irradiation represent the smallest structure dimension (below 390 nm) reported so far in our glasses, which paves the route to sub-diffraction-size fluorescent patterns by means of vortex beams.

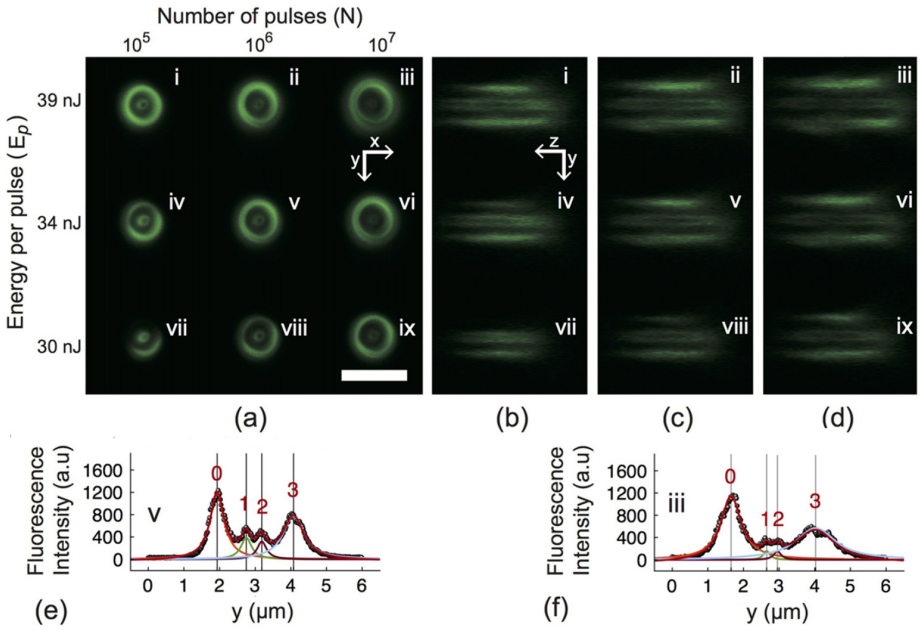

Fig. 5. Confocal image of the fluorescent patterns generated by RHC polarized LG_0^2 beams. (a) Lateral cross-sectional images in the focal plane. (b-d) Axial cross-sectional images. (e, f) Fluorescent intensity profiles of 'v' and 'iii' along the y-axis direction. Circles and lines are experimental data and Lorentzian fitting curves. Scale bars: 4 μm.

A notable difference appears for fluorescent patterns produced by RHC-polarized LG_0^1 beams [Figs. 5(a)-5(d)]. As shown in Fig. 3, the modeled on-axis laser intensity of RHC

beams is around twice that of Lin-polarized beams, which seems to be strong enough to prevent the pulse-to-pulse collapse of the inner-ring structure. Such on-axis intensity even tends to reach the photo-dissociation threshold of silver clusters, as evidenced by the drop of the fluorescent intensities of the inner-ring patterns while increasing the irradiation parameters [Figs. 5(e)-5(f)]. The inner-ring dimensions are generally larger than those from the LHC-polarized LG_0^1 beams. However, the sizes of the inner rings still tend to be moderately smaller with increasing laser irradiation and number of pulses. The dimension and the intensity of the outer patterns are similar to the ones obtained by LG_0^1 beams with LHC (Fig. 4) and Lin polarizations (as further shown in Fig. 6).

Under the same laser irradiation conditions, the Lin-polarized LG_0^1 beams lead to the experimental fluorescent patterns shown in Figs. 6(a)-6(d), depicting a similar behavior to what observed from LHC-polarized LG_0^1 in Fig. 4, with equivalent inner- and outer-ring structures. As for 'iii' of Fig. 4(a), the 'iii' of Fig. 6(a) becomes unresolved, leading to the same question whether the sub-diffraction inner-ring pattern is filled or not. It seems that the longitudinal electric field components of LG_0^1 beam with Lin and LHC polarizations are not strong here enough to make significant difference in the fluorescent patterns under the present irradiation conditions. Additionally, the inner structures look slightly better resolved with the Lin-polarized LG_0^1 beam than with the LHC-polarized beam. Even if not clear yet, this may either result from the influence of the non-zero on-axis intensity of the Lin-polarized beam at the focus, or from distinct influences of existing phase aberrations while performing laser structuring [26]. Still, this suggests that differences will rise while considering objectives with larger NA, for which the LHC polarization should provide better results since its longitudinal electric field component has an identically null on-axis value.

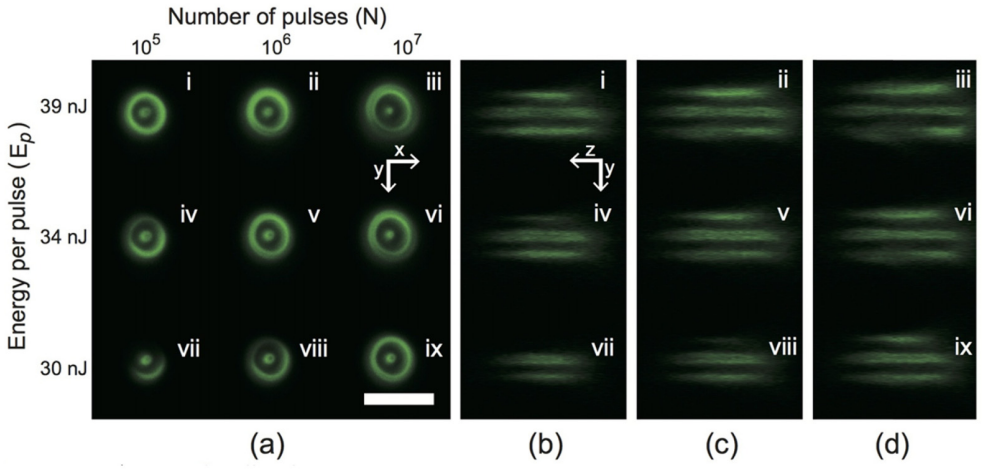

Fig. 6. Confocal image of the fluorescent patterns generated by Lin-polarized LG_0^2 beams. (a) Lateral cross-sectional images in the focal plane. (b-d) Axial cross-sectional images. Scale bars: 4 µm.

In the three considered polarization configurations, the vortex-induced fluorescent structures were obtained with laser intensities well above the laser-writing threshold. Such structures thus show a perfect permanent stability over years as well as an absence of bleaching under intense illumination, as previously reported for structures obtained by standard Gauss beam irradiation [12].

4. Conclusion

We have performed DLW by employing tightly focused femtosecond LG_0^l vortex beams with linear, left-hand and right-hand circular polarizations in a silver-containing glass. We have shown that the polarized structured vortex beams can generate unique nested double-ring fluorescent patterns. In particular, we have demonstrated that DLW with LG_0^l beams with parallel spin and orbital momenta provide a promising approach to produce super-resolution features since (i) we have generated sub-diffraction-limited fluorescent inner patterns with a 0.75 NA objective and (ii) one can expect even smaller inner structures while using objectives with higher NA because the on-axis electric field should remain identically null. This remarkable behavior results from the vortex beam induced collapse of the inner pattern close the on-axis region with no laser intensity. The dimension of the fluorescent patterns could be controlled by adjusting the irradiation parameters with the vortex beam. We believe this technique can be utilized for developing nanoscale DLW by combining with dual-color vortex beam DLW with UV co-illumination [27], since the inner or the outer structure can be selectively eliminated, leading to nanoscale fluorescent, nonlinear optical and/or plasmonic properties in such unique glass.

Funding

French State, managed by the French National Research Agency (ANR) in the frame of the "Investments for the future" program IdEx Bordeaux – LAPHIA (ANR-10-IDEX-03-02) with projects "STEDnSTRUCT" and "InPhotArch".

Acknowledgments

The microscopy was done in the Bordeaux Imaging Center, a service unit of the CNRS-INSERM and Bordeaux University, member of the national infrastructure France BioImaging. The help of Sébastien Marais is acknowledged.